Journal of Alloys and Compounds 739 (2018) 799–805

Contents lists available at ScienceDirect

Journal of Alloys and Compounds

journal homepage: http://www.elsevier.com/locate/jalcom

Exploring new methodologies for the identification of the morphotropic phase boundary region in the (BiNa)TiO_3-$BaTiO_3$ lead free piezoceramics: Confocal Raman Microscopy

Andrea Prado-Espinosa [a, *, 1], Javier Camargo [a], Adolfo del Campo [b], Fernando Rubio-Marcos [b, 1], Miriam Castro [a], Leandro Ramajo [a]

[a] Institute of Research in Materials Science and Technology (INTEMA), Juan B. Justo 4302, Mar del Plata, B7608FDQ, Argentina
[b] Electroceramic Department, Instituto de Cerámica y Vidrio, CSIC, Kelsen 5, 28049, Madrid, Spain

ARTICLE INFO

Article history:
Received 20 October 2017
Received in revised form
21 December 2017
Accepted 25 December 2017
Available online 28 December 2017

Keywords:
Piezoelectric properties
Raman spectroscopy
Lead-free piezoelectric

ABSTRACT

On ferroelectrics materials, the piezoelectric activity is enhanced near the so-called morphotropic phase boundary (MPB) separating the rhombohedral and tetragonal phases in the binary phase diagram. Here, we report the identification of the morphotropic phase boundary (MPB) region in the (1-*x*)$Na_{0.5}Bi_{0.5}TiO_3$ −*x*$BaTiO_3$ (BNT-BT) ceramic system by Confocal Raman Microscopy (CRM), emphasizing on the relationships between structure and piezoelectric properties. CRM results reveal the presence of the morphotropic phase boundary, between rhombohedral and tetragonal structures when BT concentration is close to 0.06–0.07. Raman spectroscopy can be used to rapidly identify the MPB on ferroelectric ceramics as seen in our model system (BNT-BT-based ceramics), since Raman spectra can be taken in few seconds, being then a very useful technique for material testing on industrial processes. Specifically, the methodology here showed represents an interesting way to correlate the micro and nanostructure with the properties in lead-free piezoceramics, which are controlled in part by the distribution of their different crystal phases. We believe that our results can benefit the understanding of BNT-BT ceramics expanding its applications range.

1. Introduction

The solid solutions close to the morphotropic phase transition (MPB) region, which is characterized by the coexistence of different structural phases for the same material composition, are known to exhibit high ferroelectric properties such as dielectric permittivity, piezoelectric constant, and electromechanical coupling factors [1–3]. Consequently, lead titanate-zirconate ceramics ($Pb(Ti,Zr)O_3$ - PZT), which are the most widely used piezoelectric ceramics, are formulated near the MPB region to optimize the ferroelectric properties [4,5]. However, due to the toxicity of lead, a wide range of regulations concerning environmental preservation are increasingly being introduced [6,7]. PZT ceramics are still allowed because of the lack of an adequate alternative. Therefore, research for the development of lead-free materials with properties comparable to that of PZT has been in progress for the last few years [8].

In lead free ceramic systems, bismuth-based material can potentially replace lead-based piezoelectric materials because of the presence of stereo-chemically active lone-pair electrons [9] of Bi. $Bi_{0.5}Na_{0.5}TiO_3$ (BNT) pure ceramic exhibits much weaker piezoelectric properties as compared to PZT ceramics [10,11]. To circumvent these problems, various types of compounds were added into BNT system to form solid solutions. In recent years, $Bi_{0.5}Na_{0.5}TiO_3$-$BaTiO_3$ (BNT-BT) solid solutions have received considerable attention, mainly by its interesting electromechanical properties at the morphotropic phase boundary [12,13]. The presence of MPB in different BNT-BT solutions has been reported [1,14–16], and it has been considered as one of the principal candidates for replacing of PZT. However, a necessary condition for successful synthesis of high performing materials lies in the knowledge of their physical properties, especially the peculiarities accompanying the phase transitions in BNT-based systems which are not fully understood.

* Corresponding author.
E-mail address: apespinosa@fi.mdp.edu.ar (A. Prado-Espinosa).
[1] A. Prado-Espinosa and F. Rubio-Marcos contributed equally.

https://doi.org/10.1016/j.jallcom.2017.12.308
0925-8388/

The Raman spectroscopy is a very sensitive tool to study at a local scale the structural deformations of perovskites, which are induced both by the tilting of BO_6 octahedra and by the cationic displacements, as it was well known for piezoelectrics, such as PZT, and PMN-PT systems and lead-free KNN modified ceramics [5,17] In this work, we have used a (1-*x*)$Bi_{0.5}Na_{0.5}TiO_3$-*x*$BaTiO_3$ ((1-x) BNT–xBT) based lead-free piezoelectric as a model system to investigate the evolution of the phases involved around a MPB region using Confocal Raman Microscope. For that, X-ray diffraction (XRD) and Confocal Raman Microscopy (CRM) measurements are performed in a wide range of compositions in order to determine the crystallographic evolution of the material. Further, the high sensitivity of CRM to subtle changes in the crystal symmetry allow to spatially detect the phase distribution closed to MPB in the system, providing a complementary tool to XRD for unraveling the presence of phase's coexistence. Specifically, the results indicate that the piezoelectric properties are governed by the stabilization of a Rhombohedral–Tetragonal (***R-T***) phase boundary close to room temperature which is controlled in part by the distribution of their different crystal phases.

2. Experimental details

2.1. Sample preparation

The BNT- BT ceramic samples with composition (1-x) ($Bi_{0.5}Na_{0.5}TiO_3$) - x ($BaTiO_3$) (x = 0.04, 0.06, 0.07, 0.08, 0.09) were synthesized through solid state reaction. For the synthesis of BNT, Bi_2O_3 (Aldrich 99.9%), Na_2CO_3 (Biopack 99.5%), TiO_2 (Aldrich 99%) were used. Powders were mixed and milled using zirconia balls in an alcoholic medium in a planetary mill for 3 h (Fritsch, Pulverisette 7, 1450 rpm). Powders were died and calcined at 750 °C for 2 h. For the synthesis of BT $BaCO_3$, (Biopack 99.5%), TiO_2 (Aldrich 99%) were used. Powders were mixed and milled for 3 h, and then dried and calcined at 900 °C for 2 h. For each composition, the BNT and BT resulting powders were mixed again in a planetary mill, pressed into disks and sintered at 1150 °C for 2 h.

2.2. X-ray diffraction (XRD)

Crystalline phases were characterized by X-ray diffraction (XRD) (PANalytical, X'pert Pro) The patterns were recorded over the angular range 20–80° (2θ) with a step size of 0.0334° and a time per step of 100 s, using CuKα radiation (λ = 0.154056 nm) with working voltage and current of 40 kV and 40 mA, respectively. Peaks positions were fitted assuming a Gaussian peak shape.

2.3. Electron microscopy

Microstructures were evaluated using a Field Emission Scanning Electron Microscope, FE-SEM (Hitachi S-4700) equipped with energy dispersive spectroscopy, EDS. Density values were determined using the Archimedes method.

2.4. Confocal Raman Microscope (CRM)

The Raman scattering analyses were carried out under an air atmosphere and at room temperature. The experiments were performed using a Confocal Raman Microscope coupled to an AFM (Witec alpha-300R). Raman spectra were obtained using a 532-nm excitation laser and a 100x objective lens (NA = 0.9). The incident laser power was 0.5 mW. The optical diffraction resolution of the Confocal Microscope was limited to about ~200 nm laterally and ~500 nm vertically. Raman spectral resolution of the system was down to 0.02 cm^{-1}. Samples were deposited on a microscopy glass slide and mounted on a piezo-driven scan platform having 4 nm lateral and 0.5 nm vertical positioning accuracy. For the entire compositional range under study, surface scan Raman images had 40 μm of length, 40 μm of width, 60 × 60 spectra of 0.5 s of integration time at 20 mW of laser power. Thus, the Raman image consisting of 60 × 60 pixels (3600 spectra) required ~ 30 min for acquisition of the whole surface-section. Collected spectra were analyzed by using Witec Control Plus Software, and Raman mode positions were fitted assuming a Lorentz peak shape. In addition, Raman spectra for each phase (rhombohedral, R, and the tetragonal, T, symmetry) can be compared qualitatively and quantitatively allowing to calculate the relative volume fraction of each of them, which was calculated by means Witec Control Plus Software.

2.5. Electrical properties

For the electrical measurements, ceramics were coated with a silver paste on both sides of the sintered samples. Dielectric properties were determined at different frequencies using an impedance analyzer (LCR meter HP4284A) over a frequency range of 100 Hz- 1 MHz. For the measurement of the piezoelectric constant the samples were first polarized inside a silicone bath using 2.5 kV/mm at 150 °C for 30 min, and the piezoelectric coefficients d_{33} were recorded using a quasi-static piezoelectric d_{33} m (YE2730 – Sinoceramics). The resonance and anti-resonance frequencies fr and fa were measured with an impedance analyzer (HIOKI 3535 LCR HiTESTER). The polarization–electric field (***P***–***E***) hysteresis loops were measured in a silicon oil bath using a modified Sawyer–Tower circuit.

3. Results and discussion

3.1. A classical identification approach of the morphotropic phase boundary region: XRD vs. Raman spectroscopy

A classical technique to seek structure information on lead-based piezoceramics with MPB is X-ray diffraction (XRD). The X-ray diffraction patterns of (1-x) BNT-xBT ceramics sintered at 1150 °C are shown in Fig. 1. The diffraction patterns correspond to a perovskite structure, although slight traces of a minor secondary-phase assigned to $Na_2Ti_6O_{13}$ (NTO) (JCPDS Nos. 14-0277) [18] with monoclinic structure, can be observed. This phase is more relevant in low BT concentration samples, indicating that BT affects the formation of secondary phases.

After analyzing the peaks of sintered samples located between 39°<2θ < 41° corresponding to the (003), (021) planes and 46°<2θ < 48° corresponding to the (202) plane (insert Fig. 1), the existence of a rhombohedral structure in the BNT pure can be detected, while the rest of samples display a splitting associated with the coexistence between a tetragonal symmetry, ***T***, and a rhombohedral symmetry, ***R***. Furthermore, the tetragonal symmetry, ***T***, of perovskite phase can be deconvoluted in two Gaussian peaks, (002), and (200) [6]. In addition, in these two peaks located at ~45.4 and ~45.6° (2θ) which are associated with the tetragonal symmetry, ***T***, are also detected, for samples with high BT contents (x = 0.06). At lower BT contents (x ≤ 0.06), the peaks corresponding to the (003) and (021) planes are associated with rhombohedral symmetry and are more relevant than in the ceramics with high BT contents (x = 0.06), indicating the stabilization of a rhombohedral symmetry at low BT concentrations (see insert of the Fig. 1).

Consequently, these results reveal the presence of the morphotropic phase boundary (MPB) in the BNT-BT system around a BT concentration of 6 and 7%. On the other hand, composition dependence on the volume fraction for ***R*** and ***T*** phases of each sample can be found in the Supplementary Fig. S1.

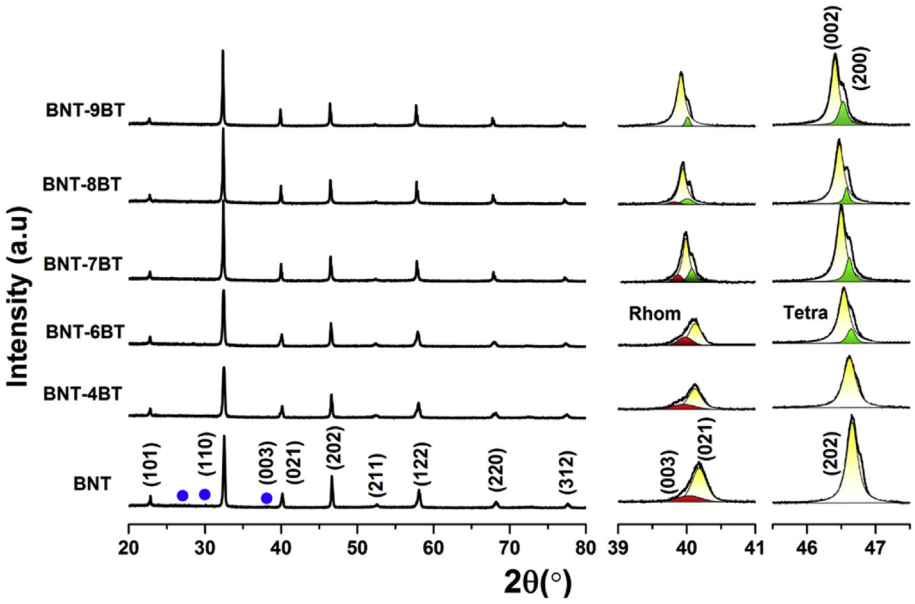

Fig. 1. Influence of BT concentration in the crystalline structure of (1-x)BNT-xBT ceramics sintered at 1150°C for 2h. The insert of each Figure shows a detail of the XRD diffraction pattern in the 2θ range 39°–41° and 45.5°–47.5° of the (1-x)BNT-xBT ceramics. These patterns are the sum of four Gaussian peaks, which are indexed as 2 tetragonal peaks (in green color) plus a rhombohedral peak (in red color) of the perovskite phase. The split peak observed for BNT at $2\theta = 46–47°$, was identified and measured in the position corresponding to $K\alpha_2$ radiation. Different peaks that are associated with the occurrence of the NTO secondary phase in BNT appear and are signaled with (•) symbol. (For interpretation of the references to color in this figure legend, the reader is referred to the Web version of this article.)

The FE-SEM micrographs of the (1-x) BNT-x BT are shown in Fig. 2a–f, while Fig. 2g–l show the average grain size (AGS). Sintered ceramics exhibit dense microstructures with low porosity, where pores are located mainly at grain boundaries and triple points. Triple points located close to 120° indicate the final stage of the sintering process where pores are removed by diffusion. Furthermore, AGS values of BNT-BT ceramics decreased with the addition of BT, which confirm influence of BT on BNT ceramics, inhibiting the grain growth [19]. Finally, Fig. 2m–r shows the energy dispersion spectrum analysis (EDS), which also reveals that all the elements are present according to their stoichiometry. EDS spectra showed a high content of titanium, sodium and barium and a good reaction between the BNT and BT attributed to the high energy the powder mixtures.

In X-ray diffraction, the system showed an increase of the tetragonal phase with the BT addition, although it should be pointed out the difficulty to fully resolve the phases ratio involved into of the MPB region (that is, in the compositional range close to $0.06 \leq x \leq 0.07$), due to the XRD peak broadening caused by both phase's coexistence and its low crystallinity. In contrast, we feel that these disadvantages can be minimized using Raman spectroscopy.

As above mentioned, BNT system has rhombohedral symmetry with a space group R3c (C^6_{3v}), meanwhile BT has tetragonal symmetry with a space group P4 mm (C^1_{4v}) at room temperature [20–22]. To verify the existence of the phase's coexistence and thus

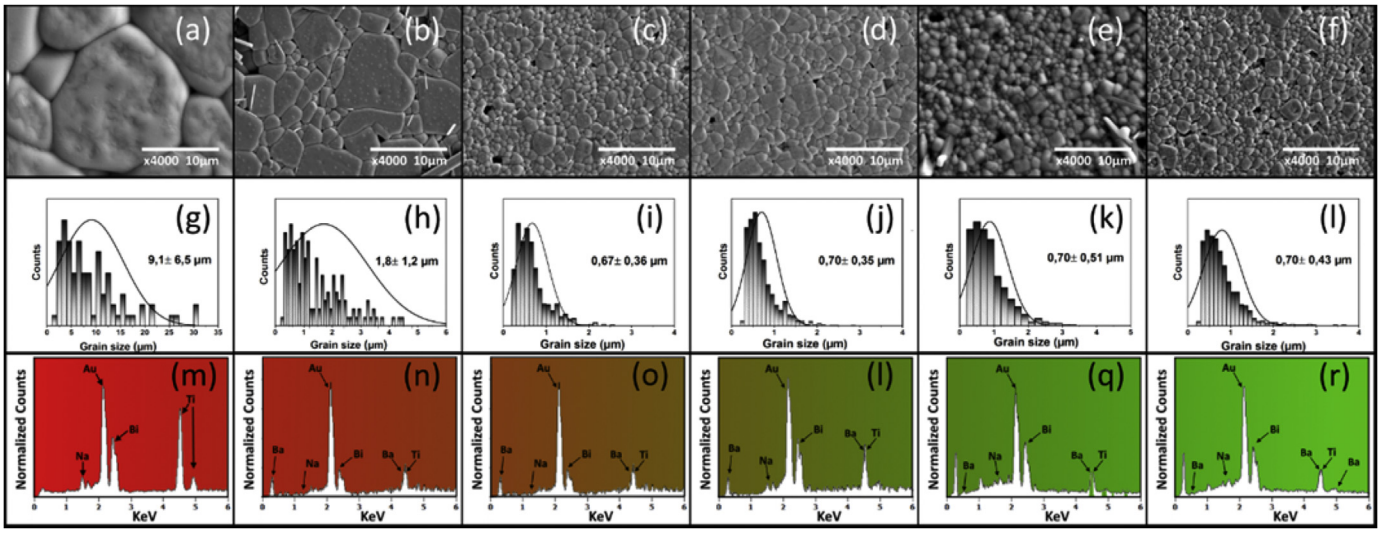

Fig. 2. FE-SEM images of (1-x) BNT-xBT (x = 0.0, 0.04, 0.06, 0.07, 0.08, 0.09) ceramics sintered at 1150°C. (Fig. 2a–f) for 2 h. The inserts of (Fig. 2g–l) show the grain-size distributions of BNT-BT ceramics. The inserts of (Fig. 2m–r) show the energy dispersion spectrum analysis (EDS).

explain the physical origin for enhanced piezoelectricity around a MPB at the macroscopic level, we have studied the nature of the crystalline symmetry of the different compositions using Raman spectroscopy.

Before discussing the spectral changes in detail, it is useful to inspect the spectral of two extreme cases corresponding to $x = 0.00$ and $x = 0.09$, which present a rhombohedral and a tetragonal symmetry, respectively**.** Fig. 3a shows the Raman spectra of the both compositions together with their spectral deconvolution into Lorentzian-shape peaks. The overall spectral signature evidences a relatively broad feature, which is in agreement with previous works [23]. The spectrum of BNT ($x = 0.00$) shows six vibration modes centered at 134, 277, 509, 580, 765 and 842 cm^{-1}, which are in agreement with reported data by other researchers [24,25]. The first mode at about 134 cm^{-1} is attributed to the Na–O bonds of the A-site vibration in the perovskite of general formula ABO_3. The second band situated at 277 cm^{-1} is associated with the vibration of the TiO_6 group and is observed in many perovskite materials [26], while the modes observed in the range between 450 and 650 cm^{-1} are controlled by vibrations involving mainly oxygen displacements. Finally, the last two modes (i.e., at 765 cm^{-1} and 842 cm^{-1}) can be correlated to the presence of oxygen vacancies [27,28]. In the extreme case, the spectra of 0.91 BNT- 0.09 BT ($x = 0.09$) show two additional peaks at ~190 cm^{-1} (signaled with asterisk symbol in the panel a of the Fig. 3) and 323 cm^{-1} (strong) compared to the peaks at 134, 277, 509, 580, 765 and 842 cm^{-1} (Raman modes assigned as 1, 2, 3, 4, 5 and 6 in the Fig. 3, respectively). Thus, the specific features allow us to establish striking differences to determine the nature of the crystalline symmetry of the different compositions.

Fig. 3b shows the Raman spectra set in the entire compositional range under study. A relevant change in the spectral feature is observed at the composition $x = 0.06$, as indicated by the dotted arrows in panel b. Specifically, the mode at low frequency (marked as 1 in Fig. 3) shifts to a lower frequency as a result of the larger mass of Ba compared to Na [29–31]. The Raman mode associated with the vibration of the TiO_6 group (assigned as 2 in Fig. 3) starts splitting into two bands (at $x = 0.06$) that shift apart each other with a further increase [24]. The two overlapping modes associated with the vibrations of the TiO_6 octahedral in the frequency range between 450 and 650 cm^{-1} show a change in the Raman intensities of the both modes as the composition increase. Therefore, considering the results of both XRD patterns and Raman spectroscopy results (See Figs. 1 and 3), three situations can be identified depending on the BT content: First, for a low doping range ($0.00 \leq x \leq 0.04$), the ceramics belong to ***R*** symmetry; secondly, it can be suggested that the MPB (***R-T*** phase boundary) lies at composition close to $x = 0.06$, and thirdly, the ***R-T*** phase boundary is suppressed in favor of a single **T** phase without the formation of a pseudo-cubic phase, with the composition increase [32,33]. Additionally, on the right of panel b and associated to each one of the structural modifications is displayed the schematic phase transition from rhombohedral **(R)** to tetragonal **(T)** phase of the (1-x)BNT-xBT system. Note that the Raman shift evolution of each mode depending on the composition can be found in the Supplementary Fig. S2.

To summarize, Raman spectroscopy can be used to rapidly identify the MPB on BNT-BT-based ceramics, since Raman spectra can be taken in some seconds, in contrast to the minutes required for a XRD measurement. Moreover, the quantity of sample required for a Raman measurement is much smaller than for a XRD measurement, being then a very useful technique for material testing on industrial processes.

3.2. Study of the phases location involved in MPB region using Raman imaging: a step forward

The identities of crystalline phases play a relevant role on the functional properties of the piezoceramics, and therefore, their identification and distribution at microscale can be used to plan new strategies in designing new materials with improved properties. For that, the Confocal Raman Microscopy (CRM) allows us acquire a high resolution of the microstructural features and an excellent spectral resolution. As has been discussed above, we can use the Raman spectra like a "*fingerprint*" in identifying the phases involved in the system. For illustrative purposes, Fig. 4a–f display

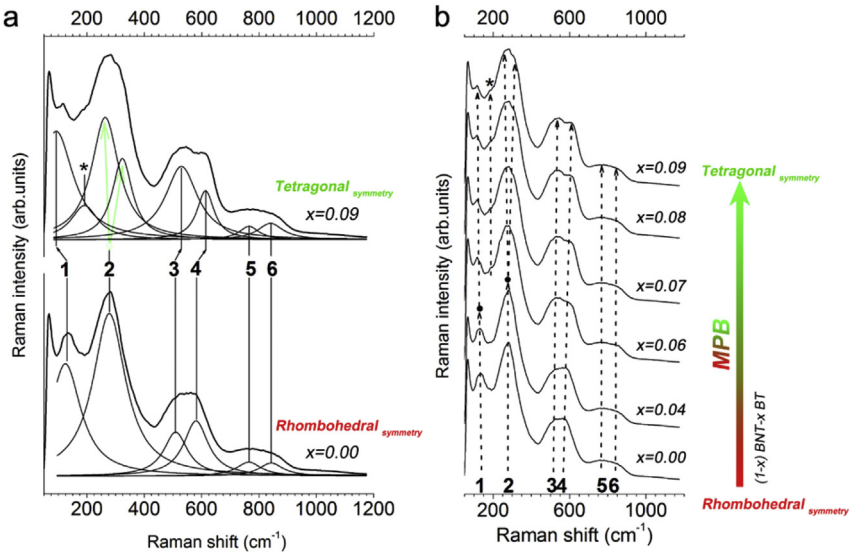

Fig. 3. Influence of BT concentration on Raman spectra of (1-x)BNT-xBT ceramics sintered at 1150°C for 2h: (a) Average Raman spectra of ceramics corresponding to $x = 0.00$ **(bottom)** and $x = 0.09$ **(top)**, which have a rhombohedral and a tetragonal symmetry, respectively. For the Rhombohedra symmetry ($x = 0.00$), its Raman spectrum is fitted as the sum of six Lorentzian modes, which are signaled in the panel a as **1**, **2**, **3**, **4**, **5** and **6**. While, for the Tetragonal symmetry (**top**) two new modes appear. **(b)** The average Raman spectra set in the entire compositional range under study. The scheme localized on right of the panels b shows the phase transition from rhombohedral (***R***) to tetragonal (***T***) phase on the (1-x)BNT-xBT system as function of the x.

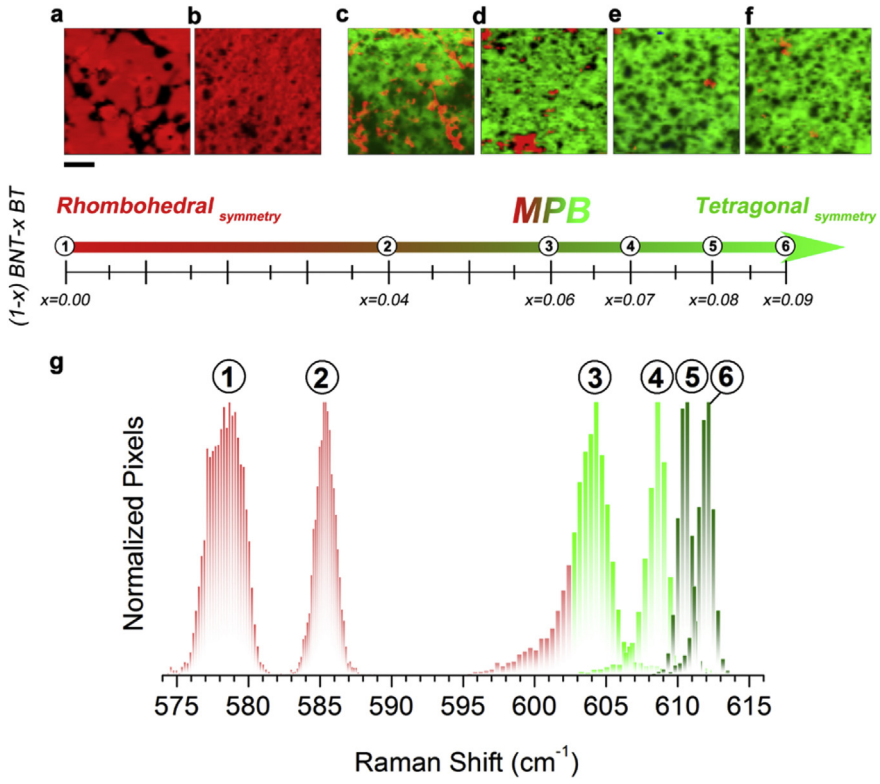

Fig. 4. A micrometric scale view of crystalline symmetry evolution of (1-x) BNT-x BT ceramics sintered at 1150 °C through confocal Raman spectroscopy: Spatial maps of the Raman signal showing the distribution of phases of the (1-x) BNT-xBT system, where the rhombohedral (***R***) symmetry and Tetragonal (***T***) are represented in red and green color, respectively. The ceramic compositions represented in the panels **a-f** are the following: **(a)** $x = 0.00$; **(b)** $x = 0.04$; **(c)** $x = 0.06$; **(d)** $x = 0.07$; **(e)** $x = 0.08$ and **(f)** $x = 0.09$. Scale bar, 10 μm. Additionally, the scheme localized at the bottom of the panels a-f represents the phase transition from rhombohedral (***R***) to tetragonal (***T***) phase on the (1-x)BNT-xBT system. **(g)** Statistical analysis of the pixel number versus mode Raman shift associated with the vibration of the TiO_6 group and localized in frequency range between ~580 and ~613 cm-1 for the rhombohedral (***R***) symmetry and Tetragonal (***T***), respectively. The ceramic compositions represented in the panel **(g)** are the following: ① $x = 0.00$; ② $x = 0.04$; ③ $x = 0.06$; ④ $x = 0.07$; ⑤ $x = 0.08$ and ⑥ $x = 0.09$. (For interpretation of the references to color in this figure legend, the reader is referred to the Web version of this article.)

the evolution of the crystalline symmetry of (1-x)BNT-x BT system as the BT content increases, where the rhombohedral ***(R)*** symmetry and Tetragonal ***(T)*** are represented in red and green color, respectively. Such spatial distribution is consistent with the fact that the structure of the solid solution transforms from ***R*** to ***T*** symmetry due to large distortion caused by BT, in good agreement with the XRD results (Fig. 1). Keeping in mind that Raman spectroscopy is also sensitive to distortion provoked by phase transitions in ceramic materials [34], the Fig. 4g monitors the distortion degree of the oxygen octahedra in the entire compositional range under study. It is displayed a statistical analysis of the pixel number versus mode Raman shift associated with the vibration of the TiO_6 group (assigned as 4 in Fig. 3). Note that a continuous increase in the Raman shift of the mode occurs when the composition increases. This behavior implies that the incorporation of BT into the BNT perovskite lattice drastically alters the observed vibration frequencies, shifting the Raman mode (assigned as 4 in Fig. 3) to higher wavenumber due to an increase in the strength constant force, caused by the shortening of the distance between B^{5+} type ions and their coordinated oxygens [35]. In fact, it is attributed to the oxygen displacements in the Ti—O bonds of the TiO_6 octahedra in the perovskite of general formula ABO_3).

3.3. Establishing relationships between the phase transition at room temperature and the functional properties

Additionally, in Fig. 5a the relative volume fraction of crystallographic phases with BT addition can be observed. A detailed inspection of Fig. 5a reveals that V_R and V_T are dependent on the BT content; indicating the involvement of tetragonal phase, this information corroborates the found in the Supplementary Fig. S1. Furthermore, it is interesting to note that the phase fraction strongly depended on the BT content. Specifically, the ceramics with $0.06 \leq x \leq 0.07$ have a room-temperature coexistence of ***R-T*** phases, being most relevant the ***T*** symmetry. Fig. 5b–c shows the d_{33} values and electromechanical coupling coefficient (k_t) of (1-x) BNT-xBT ceramics sintered at 1150 °C for 2 h. Here, it is interesting to verify that the ceramics in the compositional range between $x = 0.06$ and $x = 0.07$ simultaneously possessed a higher d_{33} of 130–165 pC/N and an adequate k_t value of 60–51%, demonstrating that piezoelectric properties are strongly depended on the coexistence of ***R-T*** phases. As it was also described in KNN-based ceramics with ***R-T*** phase coexistence [36], the construction of ***R-T*** phase coexistence induces in the system a high degree of polarization directions close to room temperature, associated with the spontaneous polarization reorientation on the $[111]_c$ and $[001]_c$ direction for rhombohedral ***(R)*** and tetragonal ***(T)*** phases, respectively. Thus, the ***R-T*** phase coexistence at room temperature produces a lattice-deformation associated with the high degree of the polarization directions that contribute to the domain mobility and therefore to the enlargement of the piezoelectric properties. In addition, these results illustrate a clear pattern: The ***R-T*** phase coexistence at room temperature affords the best piezoelectric response (see Fig. 5 and Supplementary Table S1).

Following the above analysis, the results of ferroelectric and dielectric measurements indicate that excellent properties can be

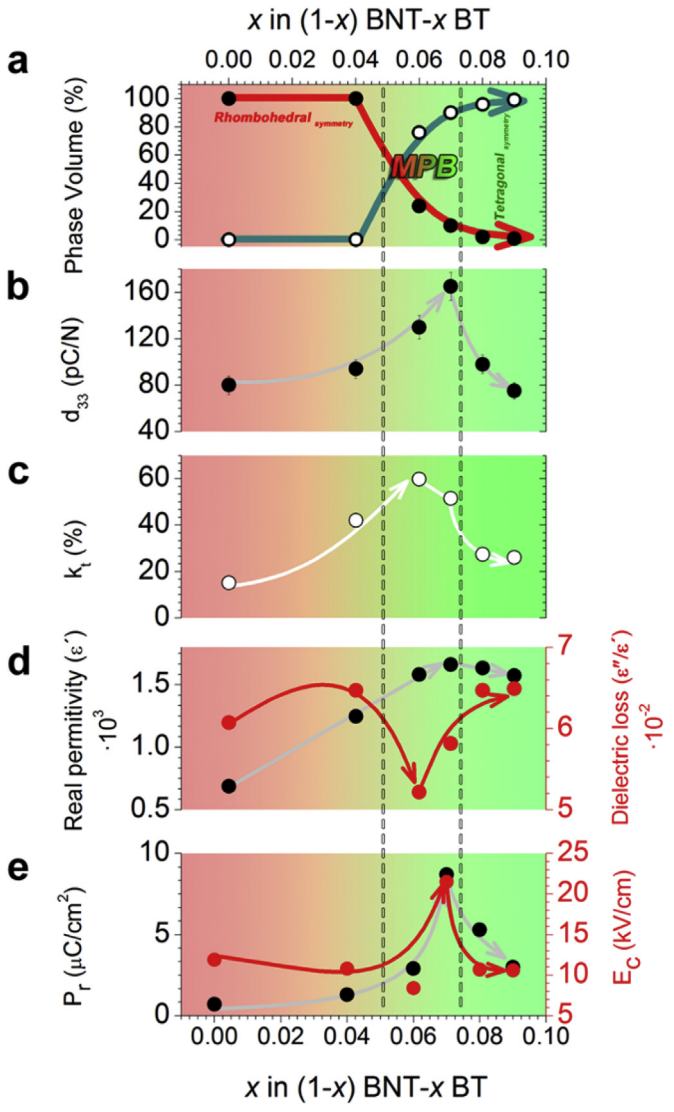

Fig. 5. Detection of high piezoelectric properties on the (1-x)BNT-x BT ceramics close to morphotropic phase boundary (MPB) region: (a) Composition dependence on the volume fraction for ***R*** and ***T*** phases, which was calculated by means Witec Control Plus Software. The red and green areas delimit the compositional regions where are located the ***R*** and ***T*** phases of the (1-x) BNT-x BT system, respectively. The white dash lines limit the morphotropic phase boundary (MPB) region involved on the (1-x)BNT-x BT system. As a comparison and to evaluate the influence of the MPB on the functional properties, the panels **(b)** and **(c)** also represent the longitudinal piezoelectric coefficients (d_{33}) and electromechanical coupling coefficient (k_t) evolution *vs.* BT content. From the Fig. 5b–c, high piezoelectric activity is observed for the phase coexistence optimal between a rhombohedral (***R***) and a tetragonal symmetry (***T***) close to $0.06 \leq x \leq 0.07$. The white dash lines limit the MPB involved on the (1-x) BNT-x BT system. The standard tolerance for the Electrical properties is ±10%. Finally, **(d)** and **(e)** represent the values of real permittivity (ε') and dielectric loss (ε'') remnant polarization (P_r), coercive field (E_c), at 10 kHz and at room temperature as a function of the BT content. (For interpretation of the references to color in this figure legend, the reader is referred to the Web version of this article.)

obtained in compositions nearby to MPB region (Fig. 5d–e). The values of remnant polarization (P_r) and coercive field (E_c) at room temperature in function of the BT content, are shows in Fig. 5e. The P_r increase significantly until reaching compositional range $x = 0.07$ of (8.7 μ/cm^2) keeping an E_c (20 kV/cm approximately). Obviously, the introduction of BT into BNT greatly lowers E_c and slightly improves P_r, this information can be corroborated in the Supplementary information Fig. S3 where it can be seen ferroelectric P-E loops of (1-x)BNT-x BT ceramics close to the morphotropic phase boundary (MPB) region. These results are in line with the Real permittivity (ε') and dielectric loss (ε'') values at room temperature in function of the BT content, shown Fig. 5d, the maximum values ε' and minimum ε'' respectively are achieved at $x = 0.07$ and $x = 0.06$ respectively. The significant enhancement in piezoelectricity of the (1-x) BNT-xBT ceramics can be attributed to the strong ferroelectricity (high P_r and low E_c) (Fig. 5e) and MPB. A low coercive field facilitates the poling process of the ceramics, and a large remnant polarization favors the piezoelectric properties; also, at the MPB the number of possible spontaneous polarization directions increases; hence the ceramics can be easily poled. Specifically, it is well-known that dielectric and ferroelectric properties determine the piezoelectric properties, remember that the d_{33} piezoelectric constant is proportional to the $\varepsilon_r P_r$ product [35,37]. As a consequence of the high values of the ε' and P_r (Fig. 5d and e), the piezoelectric properties increase close to MPB (see Supplementary Fig. S4). The high dielectric permittivity is related to the coexistence of the ***R-T*** phases, which make the system close to MBP to be more polarizable due to the existence of more directions for the polarization orientation. More importantly it provides the rotation path for the enhanced piezoelectric properties near the phase boundary [38–40]. This fact is highly remarked by the appearance of large P_r values for the compositions having rhombohedral-tetragonal coexistence at room temperature.

Summarizing, the piezoelectric properties present a clear relationship with the phase coexistence at room temperature (Fig. 5). Logically and as for P_r, the piezoelectric properties are governed by the stabilization of a Rhombohedral–Tetragonal (***R-T***) phase boundary close to room temperature, which enhances polarization process of the system. Knowing this relationship, CRM can be used to determinate these parameters and be employed as a powerful tool to in situ monitor its changes under different processing conditions.

4. Conclusions

A (1-*x*)$Na_{0.5}Bi_{0.5}TiO_3$–*x*$BaTiO_3$ (BNT-BT) system based material is used as a model to evaluate the phase's coexistence relevance to the material properties in a morphotropic phase boundary (MPB) by Confocal Raman Microscopy (CRM). Further, the high resolution of CRM to identify the phase distribution around to MPB region allow detected subtle changes in the crystal symmetry, providing a complementary tool to XRD to resolve the presence of phase's coexistence. Under the synthesis conditions (that is solid-state reaction), it is shown that the stabilization of the MBP region is located in the compositional range between $x = 0.06$ and 0.07. CRM analyses allow to determinate that two overlapping modes associated with the vibrations of the TiO_6 octahedral in the frequency range between 450 and 650 cm^{-1} show a change in the Raman intensities of the both modes as the composition increase.

The study of the phases location involved in MPB region using Raman imaging reveals a relationship between the phase transition at room temperature and the functional properties, which is attributed to the appearance of a high degree of polarization directions close to phase's coexistence (that is, the coexistence between a tetragonal symmetry, ***T***, and a rhombohedral symmetry, ***R***).

Finally, the identities of crystalline phases play a relevant role on the functional properties of the piezoceramics, and therefore, their identification and distribution at microscale can be used to plan new strategies in designing new materials with improved properties.

Conflicts of interest

The authors declare no competing financial interests.

Acknowledgements

The authors are grateful to CONICET, ANPCyT, University of Mar del Plata (Argentina) and F. R-M is also indebted to MINECO for a 'Ramon y Cajal' contract (ref: RyC-2015-18626), which is co-financed by the European Social Fund.

Appendix A. Supplementary data

Supplementary data related to this article can be found at https://doi.org/10.1016/j.jallcom.2017.12.308.

References

[1] B. Parija, T. Badapanda, S.K. Rout, L.S. Cavalcante, S. Panigrahi, E. Longo, N.C. Batista, T.P. Sinha, Morphotropic phase boundary and electrical properties of 1−x[$Bi_{0.5}Na_{0.5}$]TiO_3 −xBa[$Zr_{0.25}Ti_{0.75}$]O_3 lead-free piezoelectric ceramics, Ceram. Int. 39 (2013) 4877–4886, https://doi.org/10.1016/j.ceramint.2012.11.080.

[2] T. Takenaka, H. Nagata, Current status and prospects of lead-free piezoelectric ceramics, J. Eur. Ceram. Soc. 25 (2005) 2693–2700, https://doi.org/10.1016/j.jeurceramsoc.2005.03.125.

[3] H. Li, C. Feng, W. Yao, Some effects of different additives on dielectric and piezoelectric properties of ($Bi_{1/2}Na_{1/2}$)TiO_3–$BaTiO_3$ morphotropic-phase-boundary composition, Mater. Lett. 58 (2004) 1194–1198, https://doi.org/10.1016/j.matlet.2003.08.034.

[4] D. White, X. Zhao, M.F. Besser, X. Tan, Structure and properties of (1 − x) $Pb(Mg_{1/2}W_{1/2})O_3$ − $xPb(Zr_{0.5}Ti_{0.5})O_3$ solid solution ceramics, J. Mater. Sci. 43 (2008) 5258–5264, https://doi.org/10.1007/s10853-008-2772-1.

[5] Y. Chen, S. Xie, Q. Wang, L. Fu, R. Nie, J. Zhu, Correlation between microstructural evolutions and electrical/mechanical behaviors in Nb/Ce co-doped $Pb(Zr_{0.52}Ti_{0.48})O_3$ ceramics at different sintering temperatures, Mater. Res. Bull. 94 (2017) 174–182, https://doi.org/10.1016/J.MATERRESBULL.2017.05.045.

[6] J.-H. Cho, Y.-H. Jeong, J.-H. Nam, J.-S. Yun, Y.-J. Park, Phase transition and piezoelectric properties of lead-free ($Bi_{1/2}Na_{1/2}$)TiO_3–$BaTiO_3$ ceramics, Ceram. Int. 40 (2014) 8419–8425, https://doi.org/10.1016/j.ceramint.2014.01.051.

[7] Directive 2002/95/EC of the European parliament and of the council of 27 January 2003 on the restriction of the use of certain hazardous substances in electrical and electronic equipment, Off. J. Eur. Union (2003). L37/19–L37/37.3., (n.d.).

[8] E. Aksel, J.L. Jones, Advances in lead-free piezoelectric materials for sensors and actuators, Sensors 10 (2010) 1935–1954, https://doi.org/10.3390/s100301935.

[9] L. Ramajo, M. Castro, A. del Campo, J.F. Fernandez, F. Rubio-Marcos, Influence of B-site compositional homogeneity on properties of ($K_{0.44}Na_{0.52}Li_{0.04}$)($Nb_{0.86}Ta_{0.10}Sb_{0.04}$)$O_3$-based piezoelectric ceramics, J. Eur. Ceram. Soc. 34 (2014) 2249–2257, https://doi.org/10.1016/j.jeurceramsoc.2014.02.002.

[10] X. Ma, L. Xue, L. Wan, S. Yin, Q. Zhou, Y. Yan, Synthesis, sintering, and characterization of BNT perovskite powders prepared by the solution combustion method, Ceram. Int. 39 (2013) 8147–8152, https://doi.org/10.1016/j.ceramint.2013.03.088.

[11] C.C.C. Jin, F.F.F. Wang, L.L.L. Wei, J. Tang, Y. Li, Q.R.R. Yao, C.Y.Y. Tian, W.Z.Z. Shi, Influence of B-site complex-ion substitution on the structure and electrical properties in $Bi_{0.5}Na_{0.5}TiO_3$-based lead-free solid solutions, J. Alloys Compd. 585 (2014) 185–191, https://doi.org/10.1016/j.jallcom.2013.09.152.

[12] T. Kainz, M. Naderer, D. Schütz, O. Fruhwirth, F.A. Mautner, K. Reichmann, Solid state synthesis and sintering of solid solutions of BNT–xBKT, J. Eur. Ceram. Soc. 34 (2014) 3685–3697, https://doi.org/10.1016/j.jeurceramsoc.2014.04.040.

[13] L. Ramajo, J. Camargo, F. Rubio-Marcos, M. Castro, Influences of secondary phases on ferroelectric properties of Bi(Na,K)TiO_3 ceramics, Ceram. Int. 41 (2015) 5380–5386, https://doi.org/10.1016/j.ceramint.2014.12.100.

[14] V. Pal, O.P. Thakur, R.K. Dwivedi, Investigation of MPB region in lead free BLNT-BCT system through XRD and Raman spectroscopy, J. Phys. D Appl. Phys. 48 (2015) 55301, https://doi.org/10.1088/0022-3727/48/5/055301.

[15] P.S. Silva, J.C.C.A. Diaz, O. Florêncio, M. Venet, J.C. M'Peko, Silva, et al., Analysis of the phase transitions in BNT-BT lead-free ceramics around morphotropic phase boundary by mechanical an.pdf, Arch. Metall. Mater. 61 (2016) 17–20, https://doi.org/10.1515/amm-2016-0008.

[16] T.R. Shrout, S.J. Zhang, Lead-free piezoelectric ceramics: alternatives for PZT? J. Electroceram. 19 (2007) 113–126, https://doi.org/10.1007/s10832-007-9047-0.

[17] K. Kakimoto, K. Akao, Y. Guo, H. Ohsato, Raman scattering study of piezoelectric ($Na_{0.5}K_{0.5}$)NbO_3-$LiNbO_3$ ceramics, Jpn. J. Appl. Phys. 44 (2005) 7064–7067, https://doi.org/10.1143/JJAP.44.7064.

[18] A. Prado-Espinosa, M. Castro, L. Ramajo, Influence of secondary phases on ferroelectric properties of $Bi_{0.5}Na_{0.5}TiO_3$ ceramics, Ceram. Int. 43 (2017) 5505–5508, https://doi.org/10.1016/j.ceramint.2017.01.071.

[19] S.R. Kanuru, K. Baskar, R. Dhanasekaran, Synthesis, structural, morphological and electrical properties of NBT–BT ceramics for piezoelectric applications, Ceram. Int. 42 (2016) 6054–6064, https://doi.org/10.1016/j.ceramint.2015.12.162.

[20] J.A. Sanjurjo, E. López-Cruz, G. Burns, High-pressure Raman study of zone-center phonons in $PbTiO_3$, Phys. Rev. B 28 (1983) 7260–7268, https://doi.org/10.1103/PhysRevB.28.7260.

[21] J.A. Sanjurjo, E. López-Cruz, G. Burns, Pressure dependence of the linewidth of the soft phonons in $PbTiO_3$, Solid State Commun. 48 (1983) 221–224, https://doi.org/10.1016/0038-1098(83)90274-0.

[22] D. Rout, K.-S. Moon, V.S. Rao, S.-J.L. Kamg, Study of the morphotropic phase boundary in the lead-free $Na_{1/2}Bi_{1/2}TiO_3$-$BaTiO_3$ system by Raman spectroscopy, J. Ceram. Soc. Jpn. 117 (2009) 797–800, https://doi.org/10.2109/jcersj2.117.797.

[23] J. Anthoniappen, C.S. Tu, P.-Y. Chen, C.-S. Chen, Y.U. Idzerda, S.-J. Chiu, Raman spectra and structural stability in B-site manganese doped ($Bi_{0.5}Na_{0.5}$)$_{0.925}$-$Ba_{0.075}TiO_3$ relaxor ferroelectric ceramics, J. Eur. Ceram. Soc. 35 (2015) 3495–3506, https://doi.org/10.1016/j.jeurceramsoc.2015.05.002.

[24] H. Lidjici, B. Lagoun, M. Berrahal, M. Rguitti, M.A. Hentatti, H. Khemakhem, XRD, Raman and electrical studies on the (1−x)($Na_{0.5}Bi_{0.5}$)TiO_3−$xBaTiO_3$ lead free ceramics, J. Alloys Compd. 618 (2015) 643–648, https://doi.org/10.1016/j.jallcom.2014.08.161.

[25] I.G. Siny, E. Husson, J.M. Beny, S.G. Lushnikov, E.A. Rogacheva, P.P. Syrnikov, Raman scattering in the relaxor-type ferroelectric $Na_{1/2}Bi_{1/2}TiO_3$, Ferroelectrics 248 (2000) 57–78, https://doi.org/10.1080/00150190008223669.

[26] S. Trujillo, J. Kreisel, Q. Jiang, J.H. Smith, P.A. Thomas, P. Bouvier, F. Weiss, The high-pressure behaviour of Ba-doped $Na_{1/2}$ Bi $_{1/2}$ TiO_3 investigated by Raman spectroscopy, J. Phys. Condens. Matter 17 (2005) 6587–6597, https://doi.org/10.1088/0953-8984/17/41/027.

[27] M. Zannen, A. Lahmar, M. Dietze, H. Khemakhem, A. Kabadou, M. Es-Souni, Structural, optical, and electrical properties of Nd-doped $Na_{0.5}Bi_{0.5}TiO_3$, Mater. Chem. Phys. 134 (2012) 829–833, https://doi.org/10.1016/j.matchemphys.2012.03.076.

[28] R. Selvamani, G. Singh, V. Sathe, V.S. Tiwari, P.K. Gupta, Dielectric, structural and Raman studies on ($Na_{0.5}Bi_{0.5}TiO_3$)$_{(1-x)}$($BiCrO3$) $_x$ ceramic, J. Phys. Condens. Matter 23 (2011) 55901, https://doi.org/10.1088/0953-8984/23/5/055901.

[29] J. Suchanicz, I. Jankowska-Sumara, T.V. Kruzina, Raman and infrared spectroscopy of $Na_{0.5}Bi_{0.5}TiO_3$-$BaTiO_3$ ceramics, J. Electroceram. 27 (2011) 45–50, https://doi.org/10.1007/s10832-011-9648-5.

[30] D. Rout, V. Subramanian, K. Hariharan, V.R.K. Murthy, V. Sivasubramanian, Raman spectroscopic study of ($Pb_{1-x}Ba_x$)($Yb_{1/2}Ta_{1/2}$)O_3 ceramics, J. Appl. Phys. 98 (2005) 103503, https://doi.org/10.1063/1.2131188.

[31] M. Zannen, H. Khemakhem, A. Kabadou, M. Es-Souni, Structural, Raman and electrical studies of 2at.% Dy-doped NBT, J. Alloys Compd. 555 (2013) 56–61, https://doi.org/10.1016/j.jallcom.2012.12.002.

[32] S. Chen, X. Dong, T. Zeng, Y. Zhang, C. Mao, Thermal depolarization and ferroelectric properties of ($Bi_{0.5}Na_{0.5}$)$_{1-x}Ba_xTiO_3$ ceramics, Ferroelectrics 363 (2008) 199–208, https://doi.org/10.1080/00150190802026531.

[33] J. Kreisel, A.M. Glazer, G. Jones, P.A. Thomas, L. Abello, G. Lucazeau, An x-ray diffraction and Raman spectroscopy investigation of A-site substituted perovskite compounds: the ($Na_{1-x}K_x$)$_{0.5}$ $Bi_{0.5}TiO_3$ ($0<x<1$) solid solution, J. Phys. Condens. Matter 12 (2000) 3267–3280, https://doi.org/10.1088/0953-8984/12/14/305.

[34] X. Vendrell, J.E. García, E. Cerdeiras, D.A. Ochoa, F. Rubio-Marcos, J.F. Fernández, L. Mestres, Effect of lanthanide doping on structural, microstructural and functional properties of $K_{0.5}Na_{0.5}NbO_3$ lead-free piezoceramics, Ceram. Int. 42 (2016) 17530–17538, https://doi.org/10.1016/j.ceramint.2016.08.066.

[35] L. Ramajo, M. Castro, A. del Campo, J.F. Fernandez, F. Rubio-Marcos, J. Holc, J.F. Fernández, M. Nakamura, Revealing the role of cationic displacement in potassium–sodium niobate lead-free piezoceramics by adding W^{6+} ions, J. Mater. Chem. C 3 (2015) 4168–4178, https://doi.org/10.1039/C4TC02908A.

[36] F. Rubio-Marcos, R. López-Juárez, R.E. Rojas-Hernandez, A. del Campo, N. Razo-Pérez, J.F. Fernandez, Lead-free piezoceramics: revealing the role of the rhombohedral–tetragonal phase coexistence in enhancement of the piezoelectric properties, ACS Appl. Mater. Interfaces 7 (2015) 23080–23088, https://doi.org/10.1021/acsami.5b06747.

[37] B. Zhang, J. Wu, X. Cheng, X. Wang, D. Xiao, J. Zhu, X. Wang, X. Lou, Lead-free piezoelectrics based on potassium–sodium niobate with Giant d_{33}, ACS Appl. Mater. Interfaces 5 (2013) 7718–7725, https://doi.org/10.1021/am402548x.

[38] B. Noheda, D.E. Cox, G. Shirane, J.A. Gonzalo, L.E. Cross, S.-E. Park, A monoclinic ferroelectric phase in the $Pb(Zr_{1-x}Ti_x)O_3$ solid solution, Appl. Phys. Lett. 76 (1999) 2059–2061, https://doi.org/10.1063/1.123756.

[39] R.E. Cohen, H. Fu, Polarization rotation mechanism for ultrahigh electromechanical responsein single-crystal piezoelectrics, Nature 403 (2000) 281–283, https://doi.org/10.1038/35002022.

[40] B. Noheda, D.E. Cox, G. Shirane, S.-E. Park, L.E. Cross, Z. Zhong, Polarization rotation via a monoclinic phase in the piezoelectric 92%$PbZn_{1/3}Nb_{2/3}O_3$-8% $PbTiO_3$, Phys. Rev. Lett. 86 (2001) 3891–3894, https://doi.org/10.1103/PhysRevLett.86.3891.